Supporting Information for

Reconstruction, Analysis, and Segmentation of LA-ICP-MS Imaging Data using Python for the Identification of Sub-Organ Regions in Tissues
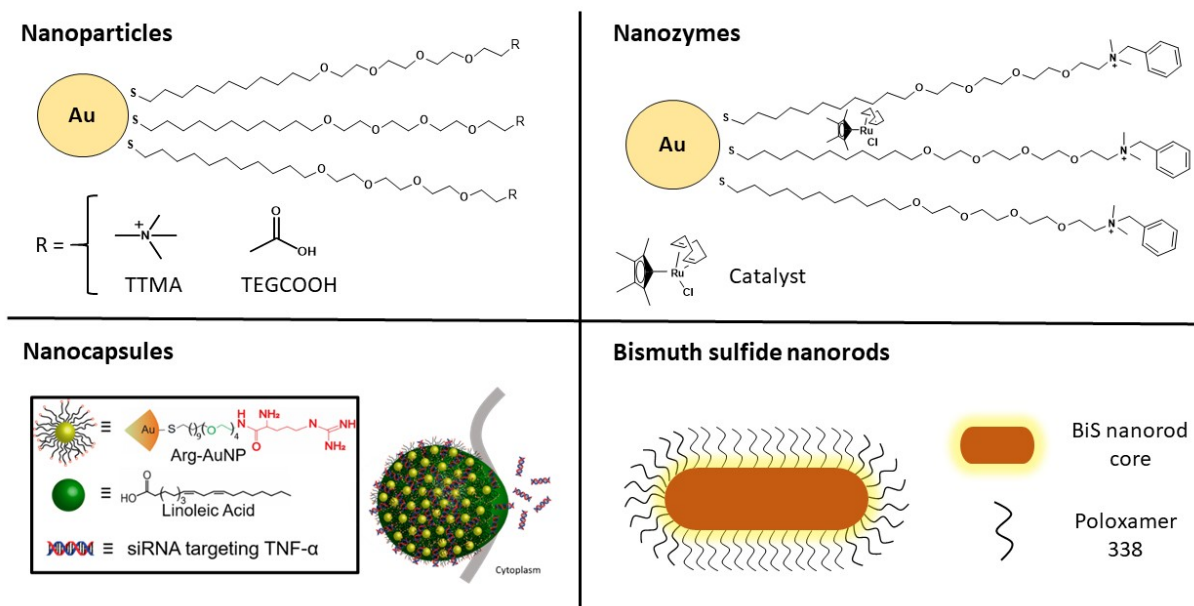
Contents:

Fig. S1. Description of the nanomaterials used in this work. Nanoparticles, nanozymes, nanocapsules and bismuth sulfide nanorods.
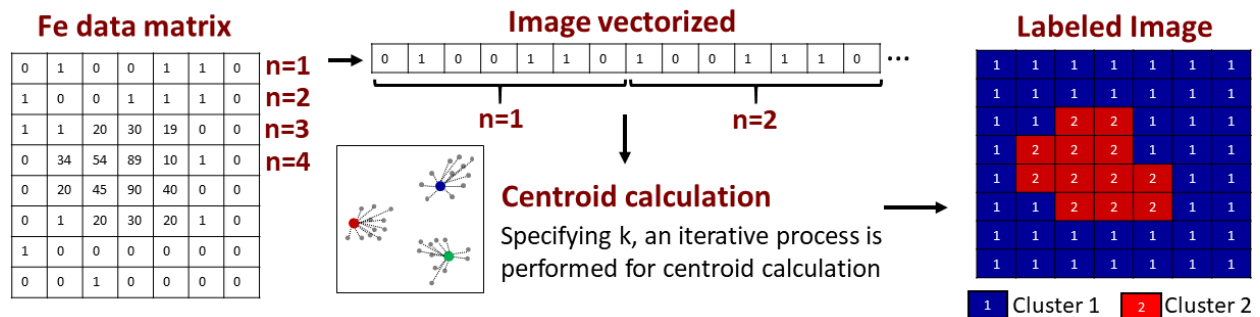
Fig. S2. k-means clustering process. The data matrix is vectorized, k centroids are calculated in an iterative process until the overall error remains constant, and finally the labeled image is reshaped.
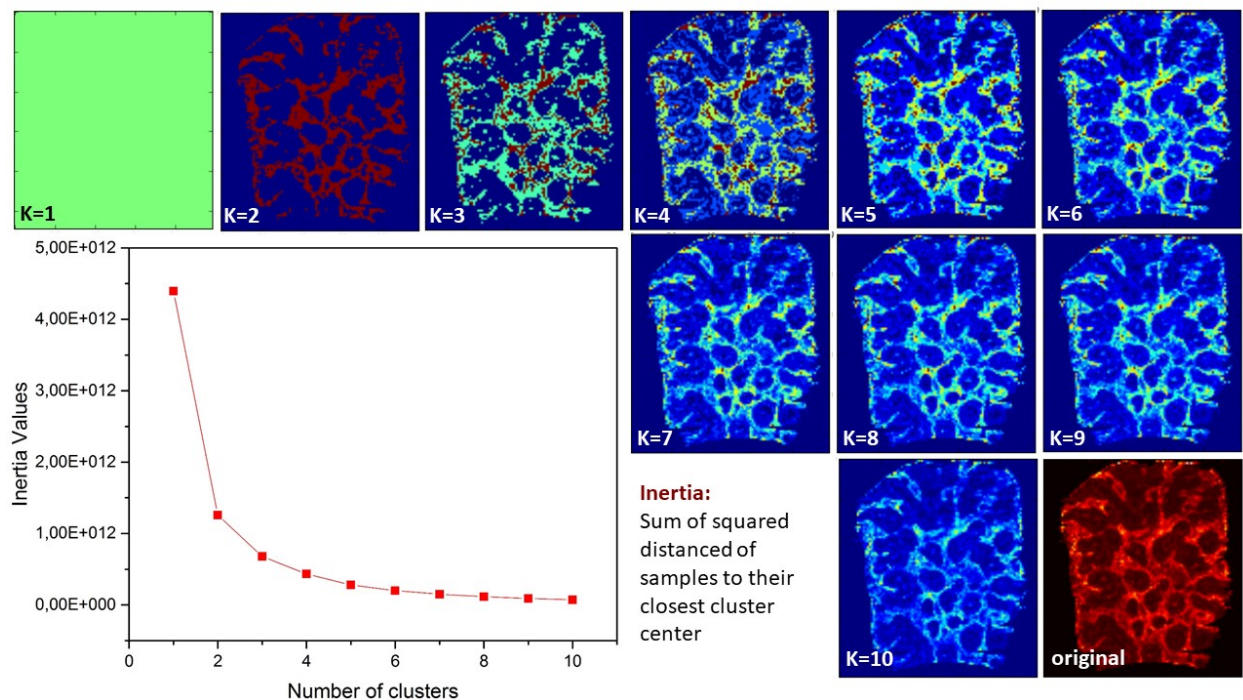

Fig. S3. Example of the use of the elbow method for clustering of an image. Inertia values were calculated for each number of clusters for the same image. The ideal value in these data corresponds to k=2 or k=3. The elbow method is an empirical approach that allows the data analyst to select the optimal number of clusters from a given data set or image. For this purpose, k-means clustering is performed on the same data set, for different k values, and inertia values are calculated. The inertia values for each dataset correspond to the sum of squared distances of every sample to their closest cluster center. Once inertia values are calculated, they are plotted against the number of clusters to find the "elbow" or inflection point of the curve.
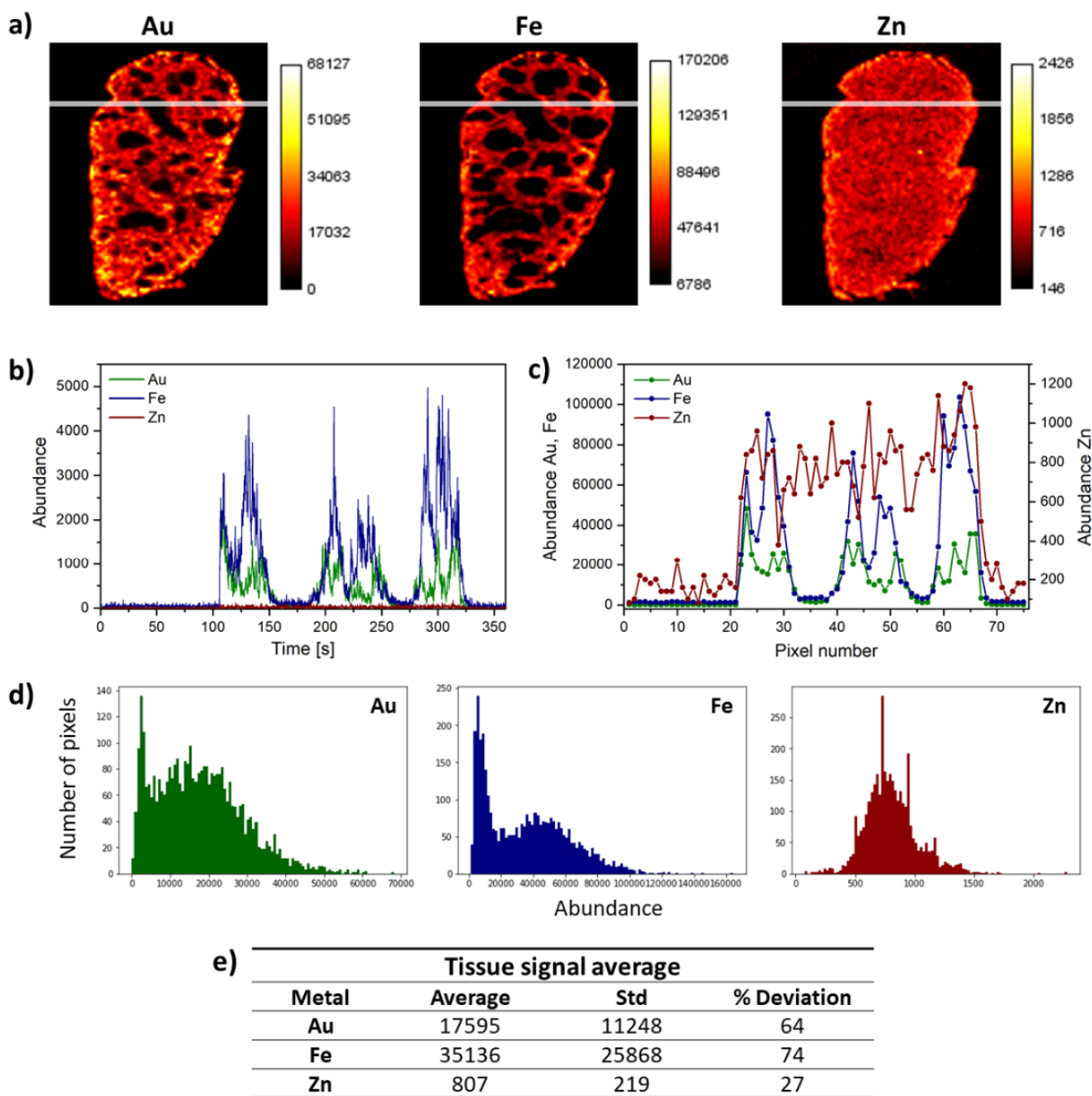
Tissue signal average			
Metal	**Average**	**Std**	**% Deviation**
Au	17595	11248	64
Fe	35136	25868	74
Zn	807	219	27

Fig. S4. Elemental distribution of Au, Fe and Zn in a spleen tissue from a mouse injected with Au nanoparticles. The figure show: a) Spleen images of Au, Fe and Zn. b) Raw signal data for the ablation of one of the tissue lines analyzed in LA-ICP-MS. The line is shown in gray over the LA-ICP-MS image. c) Data binning every 33 points is performed on the raw signal to obtain a pixel size of 50 μm x 50 μm. d) Histograms for the distribution of Au, Fe and Zn signals found in the tissue. e) Average Au, Fe and Zn signals, standard deviations, and % deviations across the tissue. One key conclusion from these data is that the Zn signal is relatively constant across the tissue.
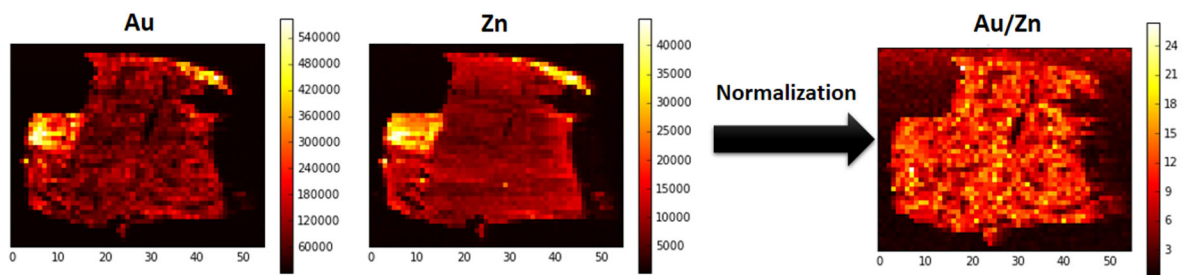
Fig. S5. Normalization of the Au distribution using the Zn data from a liver tissue from a mouse injected with Au nanocapsules. The tissue is folded on the upper left side of the tissue.
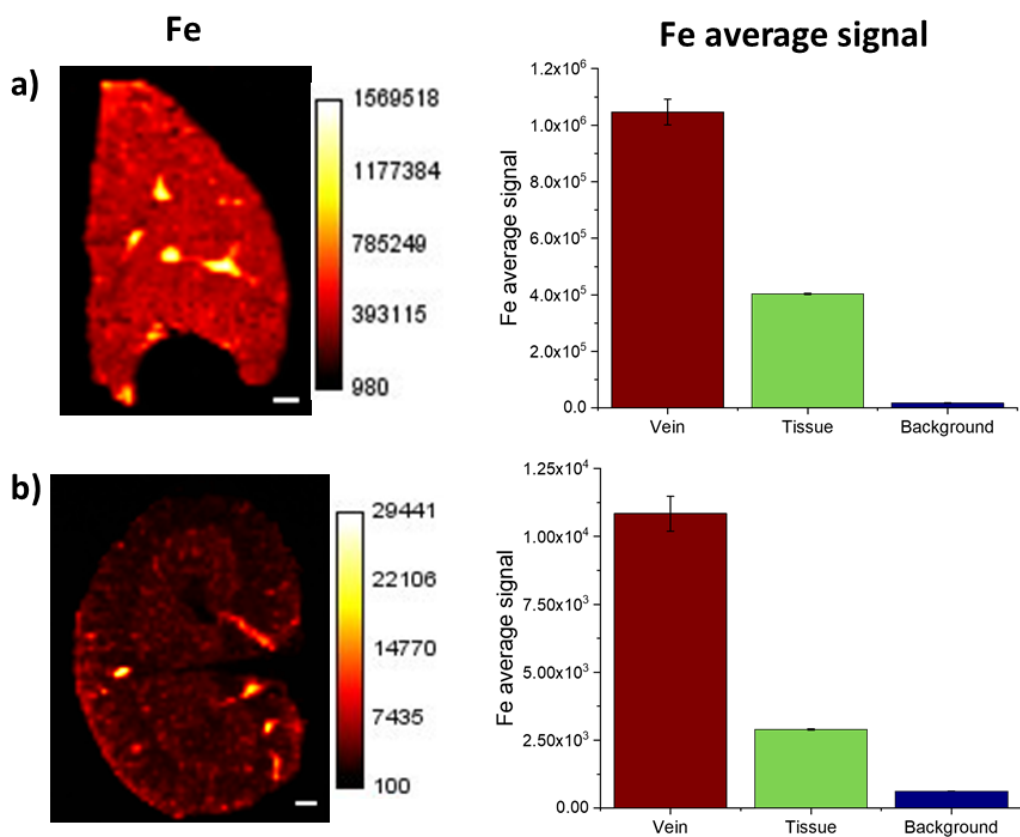

Fig. S6. Distributions of Fe signals in different suborgan regions for: a) liver section from a mouse injected with TTMA Au nanoparticles and b) a kidney section from a mouse injected with TEGCOOH Au nanoparticles.
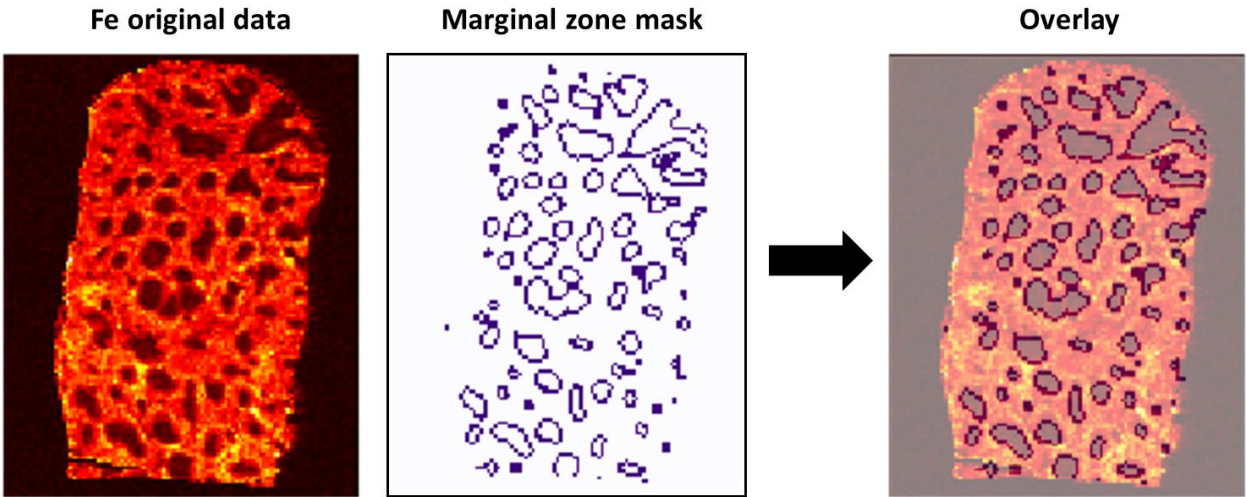
Fe original data **Marginal zone mask** **Overlay**

Fig. S7. Overlay of the Fe distributions in the LA-ICP-MS data from a spleen tissue with the marginal zone mask calculated through multi-metal segmentation and neighboring pixel evaluation shown in Figure 6 of the main text.
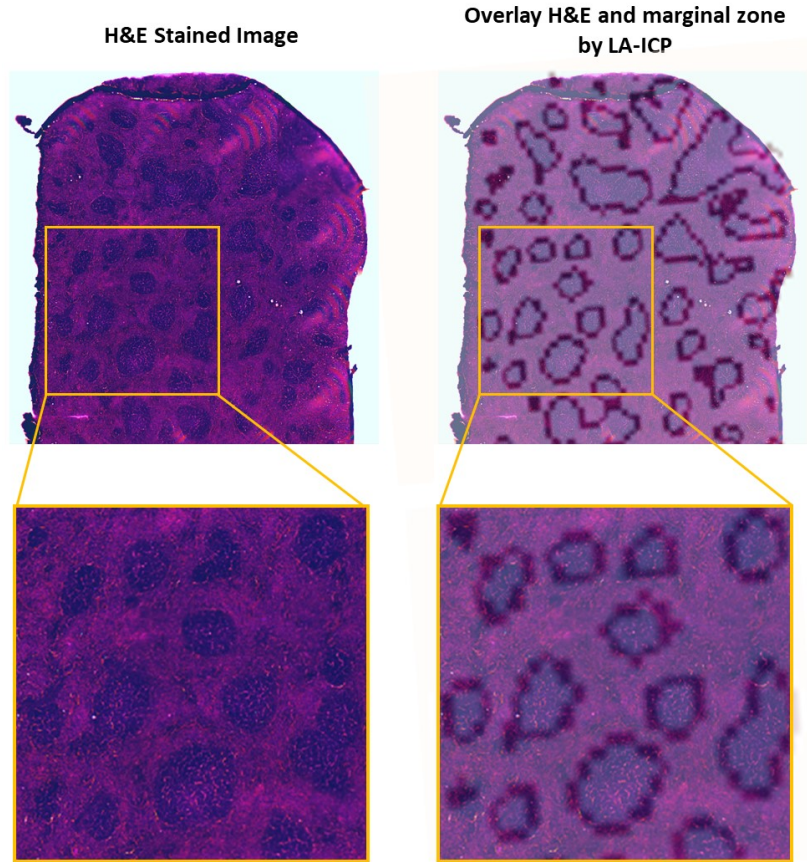

H&E Stained Image **Overlay H&E and marginal zone by LA-ICP**

Fig. S8. H&E stained image (left), and an overlay of the H&E stained and segmented images (right), demonstrating the success of the multi-metal image segmentation and pixel evaluation for the differentiation of the different regions of the spleen.
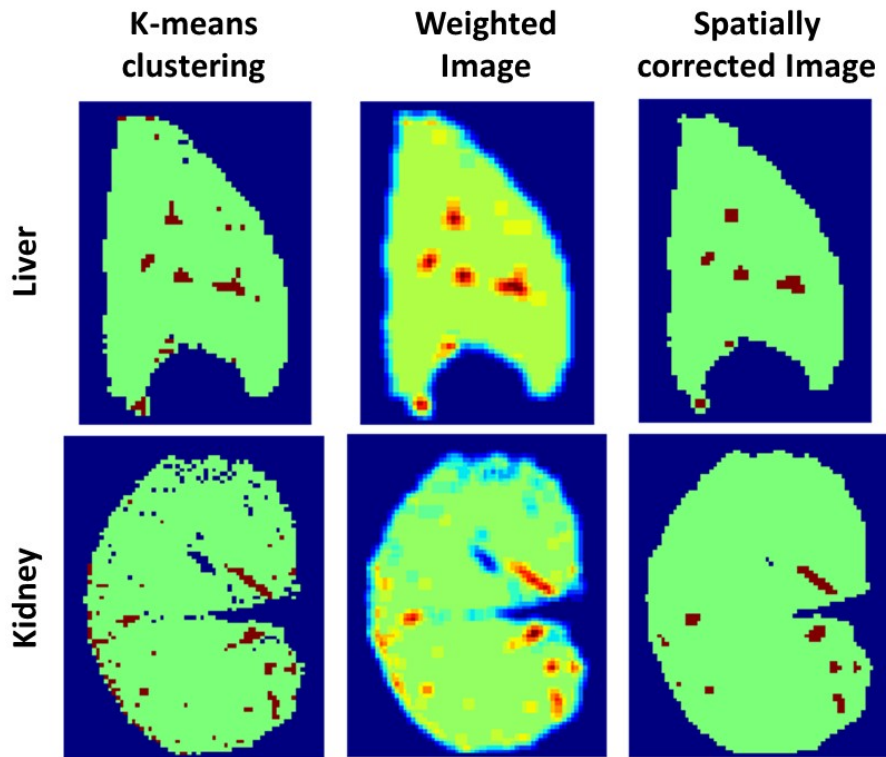
Fig. S9. Effect of neighboring pixel evaluation in the spatial awareness correction of the liver and kidney images from Figure 5 in the main text. In addition to boundary pixel classification, the neighboring-pixel evaluation also introduces spatial awareness to the multi-metal segmentation in k-means clustering. This figure shows the benefits of adding spatial awareness to the image segmentation. If we consider the k-means clustered liver image (top right), we find several 'red spots' that are incorrectly classified as blood vessels. Upon spatially correcting the liver image (top right), the wrongly classified blood vessels disappear. Similarly, if we compare the k-means clustered kidney image (bottom left) with the spatially corrected kidney image (bottom right), we can see that the k-means clustered image show some pixels that are wrongly classified as background (blue dots inside the kidney tissue). After performing the neighboring-pixel evaluation, the majority of the wrongly classified pixels are properly reclassified (in green), because a spatial awareness factor is introduced.
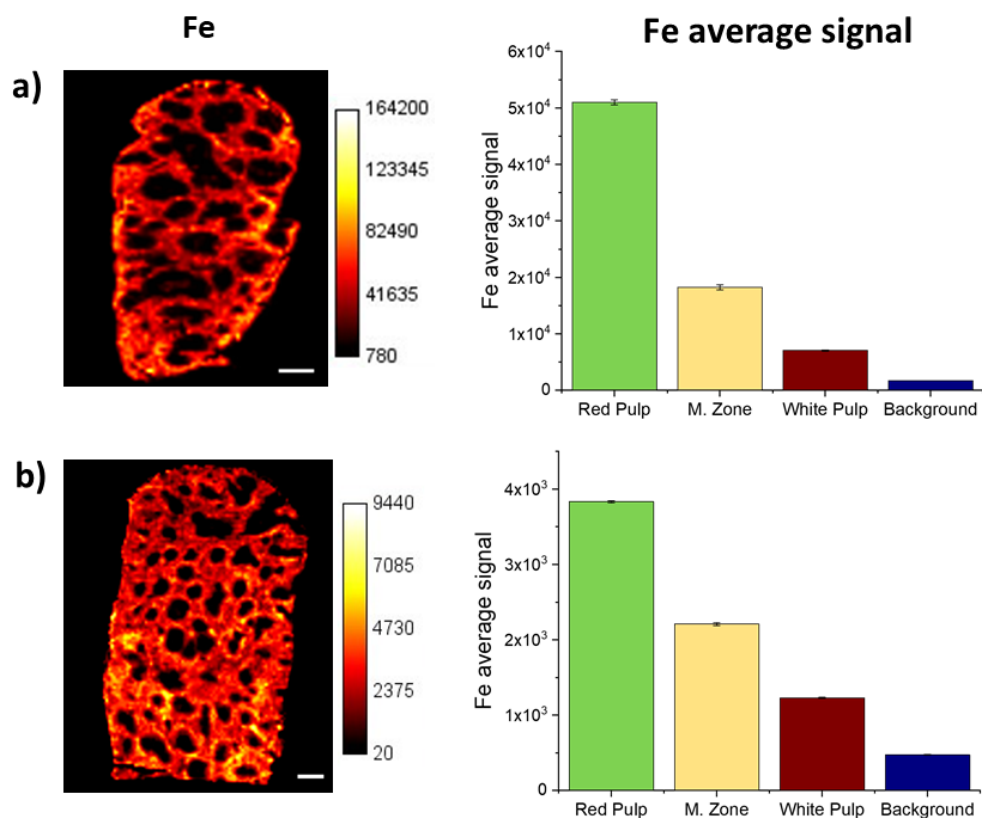
Fig. S10. Distributions of Fe signals in different suborgan areas for spleen tissue from: a) a mouse injected with Au nanoparticles and b) a mouse injected with bismuth nanorods.
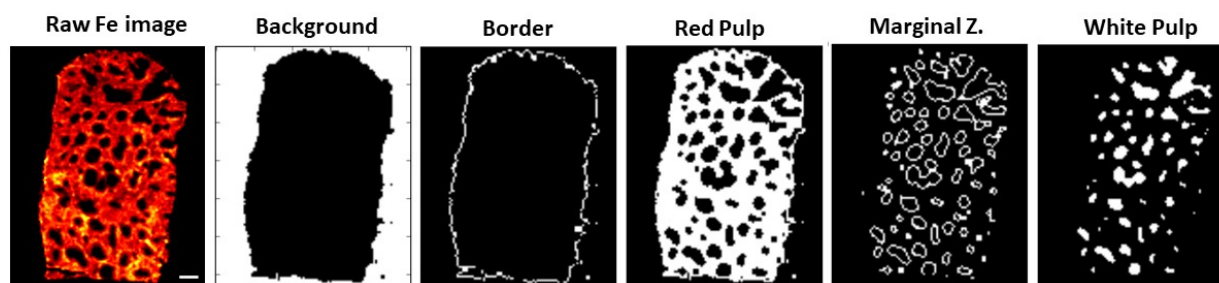

Fig. S11. Spatial mask images for a spleen from a mouse injected with bismuth sulfide nanorods. Fe-based classification through k-means clustering allows the creation of different spatial masks that facilitate determination of the amount of bismuth in each sub-organ region. Scale bar correspond to 500 μm.